Nematic Solvation of Segmented Polymer Chains

ARTICLE *in* NANO LETTERS · OCTOBER 2005

Impact Factor: 13.59 · DOI: 10.1021/nl051108l · Source: PubMed

5 AUTHORS, INCLUDING:

Dehong Hu
Pacific Northwest National Laboratory
89 PUBLICATIONS **4,679** CITATIONS

NANO LETTERS

2005
Vol. 5, No. 9
1757−1760

Nematic Solvation of Segmented Polymer Chains

S. Link,[†] D. Hu,[‡] W.-S. Chang,[†] G. D. Scholes,[§] and P. F. Barbara*,[†]

Center for Nano- and Molecular Science and Technology, University of Texas at Austin, Austin, Texas 78712, Pacific Northwest National Laboratory, P.O. Box 999, Richland, Washington 99352, and Lash-Miller Chemical Laboratories, 80 St. George Street, University of Toronto, Toronto, Ontario M5S 3H6, Canada

Received June 12, 2005; Revised Manuscript Received July 19, 2005

ABSTRACT

We examine the effect of polymer chain segmentation on the recently discovered ability of nematic solvents to *elongate and align polymer chain solutes*. Coordinated single molecule spectroscopy and beads-on-a-chain simulations are used to study the orientational and conformational order of a series of segmented conjugated polymers, dissolved in the nematic liquid crystal 5CB. The order parameters for alignment and elongation are both observed to decrease with increasing segmentation, reflecting an interplay among conformational entropy, solvation anisotropy, and bending energy of the chain.

Onsager[1] first predicted that in a binary "solution" of long and short rods, the long rods experience an enhanced alignment in the nematic environment of the shorter rods.[2] The first compelling experimental evidence for this type of "anisotropic solvation" has only been reported recently for single polymer molecules.[3,4] Large single semiflexible biopolymers in the nematic phase of rodlike *fd* virus were visualized directly by fluorescence imaging[3] and found to undergo a coil−rod transition at the isotropic−nematic phase transition. Independently, polarization sensitive single molecule spectroscopy (SMS) revealed that conjugated polymer (MEH−PPV) chains dissolved in a single liquid crystal of 5CB are nearly perfectly aligned with the nematic director of the liquid crystal (LC).[4] Here using SMS and beads-on-a-chain simulations, we explore the effect of polymer chain segmentation on the alignment and elongation in a nematic environment for a series of conjugated MEH−PPV polymers for which synthetic introduction of single bonds at various double bond locations create a controllable number of rigid polymer segments separated by single bonds. For chains with only a few segments, anisotropic solvation due to the nematic solvent is observed to highly elongate the chains. As the number of polymer segments is increased, the chains become less elongated due to an interplay among conformational entropy, anisotropic solvation, and the bending energy of the polymer. In addition, highly segmented chains in nematic solvents are observed by simulation to possess low-energy "hairpin turn" defects that can dramatically decrease the extension ratio without a significant energy penalty from solvation or bending.

Polymer chains of three different MEH−PPV compounds, denoted by M*X* (i.e., M98, M70, and M45, where *X* is 100 minus the percentage of tetrahedral defects[5]) were investigated. The chains were isolated at high dilution in a single domain nematic 5CB liquid crystal[4,6] (2.5 cm × 2.5 cm × 50 μm) at 22 °C. Data were acquired in a home-built confocal microscope in either "emission mode" (i.e., two orthogonally polarized detector systems each with an APD detector), or "excitation mode" (i.e., one unpolarized detection channel but two orthogonally polarized excitation beams that were synchronously chopped at 10 kHz).

Individual polymer molecules diffusing through the excitation volume gave rise to fluorescence bursts. For emission mode the polarization ratio was determined for each burst as $P = (I_{y,\mathrm{em}} - I_{x,\mathrm{em}})/(I_{y,\mathrm{em}} + I_{x,\mathrm{em}})$, where $I_{x,\mathrm{em}}$ and $I_{y,\mathrm{em}}$ are the *x* and *y* polarized florescence intensities. For excitation mode $P = (I_{y,\mathrm{exc}} - \mathrm{I}_{x,\mathrm{exc}})/(I_{y,\mathrm{exc}} + I_{x,\mathrm{exc}})$, where $I_{x,\mathrm{exc}}$ and $I_{y,\mathrm{exc}}$ are the fluorescence intensities of the single APD detector, with *x* and *y* polarized excitation. Histograms of *P* were generated from several thousand bursts and are shown in Figure 1 for M98, M70, and M45. Each panel shows a histogram for three sample orientations where the LC director is either aligned along the *x*-axis giving rise to negative *P* values, aligned along the *y*-axis giving rise to positive *P* values, or aligned at an angle of 45° to the *x*-axis leading to *P* values centered around zero.

Single conjugated polymer chains are well described as a multichromophoric system in which a chromophore consists of 10−15 repeat units.[7] The *P* values are a measure of the

[†] University of Texas at Austin.
[‡] Pacific Northwest National Laboratory.
[§] University of Toronto.

10.1021/nl051108l CCC: $30.25
Published on Web 07/27/2005

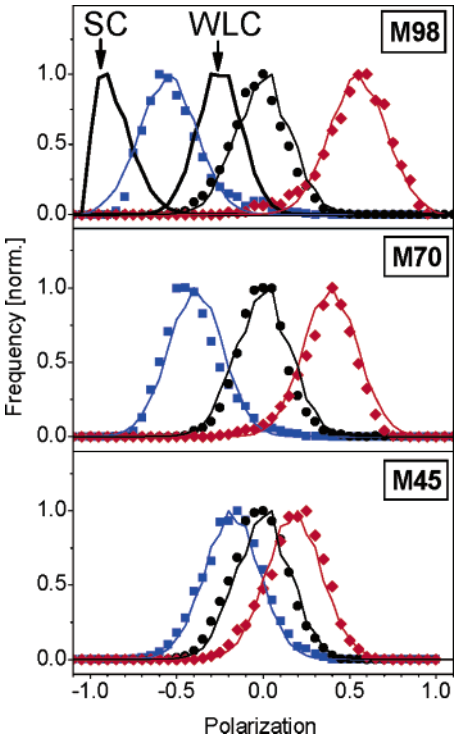

Figure 1. Experimental polarization histograms (symbols) for M98 (top), M70 (middle), and M45 (bottom) and fits (lines). Distributions collected in excitation mode (not shown) were indistinguishable from the emission mode for M98. The two limiting cases of a straight chain (SC) and a wormlike chain (WLC) with the appropriate 2% of defects are included as solid lines (top). The excitation wavelengths were 457 nm for M45 and 488 nm for M98 and M70. The average excitation power was 100−200 nW.

"polarization" of the molecular transition dipole for each chain

$$P_{\text{chain}} = \left(\sum_i {\mu_{ix'}}^2 - \frac{1}{2}\sum_i ({\mu_{iz'}}^2 + {\mu_{iy'}}^2)\right) / \left(\sum_i {\mu_{ix'}}^2 + \frac{1}{2}\sum_i ({\mu_{iz'}}^2 + {\mu_{iy'}}^2)\right) \quad (1)$$

where $\vec{\mu}_i$ is the transition dipole of the ith segment and cylindrical molecular symmetry is assumed. Model calculations (described below) demonstrate that, due to the relatively low free energy cost of aligning the chains along the nematic director, the chains are well aligned with an orientational order parameter S_O which approaches unity and far exceeds the 0.48 value for 5CB[8] (i.e., $S_O = \langle {}^3/_2 \cos^2 \alpha - {}^1/_2 \rangle$ where α is the tilt angle between the major axis of the chain and the director). In analogy to the molecular orientational order parameter, S_O, a conformational order parameter can be defined as, $S_C = \langle {}^3/_2 \cos^2 \beta - {}^1/_2 \rangle$ where β is the angle between each segment and the polymer principle internal axis (x'), i.e., the direction of maximum orientation.

The alignment of a long rigid rod present at low mole fraction in the nematic phase of short rods can be understood through an extension of Onsager's description of the orientation-dependent excluded volume of rod-shaped molecules.[2] However, the alignment of a segmented polymer is a considerably more complex problem. For example, the free energy contribution from each segment along the chain can be summed, but the distribution functions describing their orientations are entangled because the segments are linked. By investigating a series of polymers with varying sizes of rigid segments, we are able to obtain insights into the synergistic orientation of the segments. To elucidate a meaningful structural model that reflects our observations, we need to define two kinds of order parameters: one for the polymer, which is essentially an ensemble of segments, S_O, and one for the orientation distribution of segments within the polymer chain, S_C.

It is interesting to compare the experimental M98 results (~423 repeat units and only 8 defects per chain on average) with theoretical predictions for two limiting cases, i.e., a fully elongated, rigid straight chain (SC) and a wormlike chain (WLC) with the appropriate 2% of defects (2 defects per 100 beads), as shown in Figure 1. The theoretical predictions include effects due to photon shot-noise and the high numerical aperture of the objective.[9] The experimental M98 values fall intermediate between the fully elongated ($P_{\text{chain}} = 1$) and the WLC isotropic chain limits. The decrease in P values with increasing number of segments along the polymer chains demonstrates that segmentation resists the elongation process. The excitation (not shown) and emission polarization distributions for M98 are indistinguishable, which is consistent with the expectation that the observed P values are not distorted by energy transfer effects.[10] It should be emphasized that this analysis demonstrates that the observed P values are significantly smaller than the actual P_{chain} values due to the high numerical aperture of the objective that collects and excites with z-component light, lowering the detected polarization in the emission-mode and excitation-mode experiments, respectively.

Further insight into the anisotropic solvation of segmented polymer chains was obtained by Monte Carlo (MC) simulations by adopting our previous model[11,12] for segmented conjugated polymers, i.e., a chain of 100 hard beads connected by bonds with a chain bending energy, $E_{\text{bend}} \sim 10 k_B T \text{ rad}^{-2} \cdot \psi^2$, where ψ is the angle difference from the equilibrium bond angle (180° for normal bonds and 109.5° for the tetrahedral defects that join each segment). The model was adapted by introducing a mean-field anisotropic solvation potential[13] per repeat unit, V_{RU}, of the polymer chain

$$V_{\text{RU}}(\chi) = -\frac{3}{2} \nu_{\text{RU}} \cos^2 \chi \left\langle \frac{3}{2} \cos^2 \gamma - \frac{1}{2} \right\rangle \quad (2)$$

where υ is the solute−solvent intermolecular interaction strength, χ is the angle of the each repeat unit (and associated segment) relative to the nematic director, and γ is the angle of each LC solvent molecule relative to the director. Since the polymer chains are highly dilute, we use the order parameter of 5CB for the required value in eq 2, i.e., $\langle {}^3/_2 \cos^2 \gamma - {}^1/_2 \rangle = 0.48$.[8] Furthermore, since a MEH−PPV repeat unit is similar in chemical properties to 5CB but roughly $^1/_3$ smaller in size, we use $\sim {}^1/_3$ of the υ value for 5CB, i.e., $\upsilon_{5\text{CB}} = 4.6 k_B T$ for 5CB and $\upsilon_{\text{RU}} = 1.4 k_B T$ for each

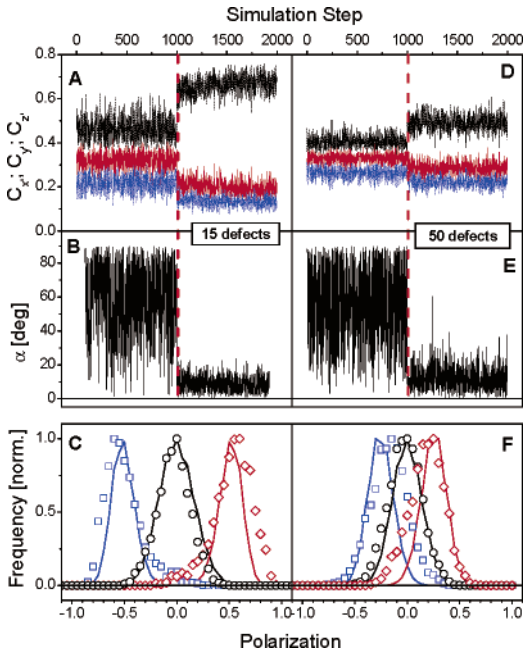

Figure 2. Normalized absorption cross sections along the three principal axes of the conformation (A, D) and orientation angle α (B, E) versus MC simulation step for a polymer with 15 (left) and 50 defects (right). (C, E) Polarization histograms calculated from the MC conformations (lines) compared to the measured polarization distribution (symbols) for M98 (left) and M45 (right).

bead length on the chain. In addition, the intrachain interaction potential was assumed to be repulsive, consistent with SMS polarization selection experiments that indicate that MEH−PPV adopts an "uncollapsed" conformation in 5CB.[10]

Figure 2 illustrates simulated normalized absorption cross sections (A, D) along the three principal axes of the conformation and orientation angle α (B, E) versus MC simulation step for a polymer with 15 and 50 defects. Initially the LC anisotropic solvation energy is set to zero and is turned on after 1000 steps. Upon its inclusion, the shape of the molecule becomes more anisotropic (elongated), observed as an increase in the absorption cross section of the major axis, and a corresponding decrease in that of the two minor axes. The mean field potential also forces the major axis of the molecule to align with the LC nematic director. This is further illustrated in Figure 3, which shows two typical conformations of a 100-segment homopolymer with 15 defects without (A) and with (B) the LC potential. The nematic director is parallel to the *x*-axis. Correspondingly, (C) and (D) show typical conformations for a chain with 50 defects.

Parts C and F of Figure 2 show a comparison of the simulated and experimentally observed polarization distributions demonstrating good qualitative agreement. The number of defects per chain was adjusted arbitrarily to get good agreement between the simulated and observed *P* data. It is not surprising that the number of defects in the best-fit simulation differs significantly from the actual number of defects, considering the simplicity of the model and that it was necessary due to limited computational resources to simulate chains with a much smaller number of repeat units compared to the experimental chains.

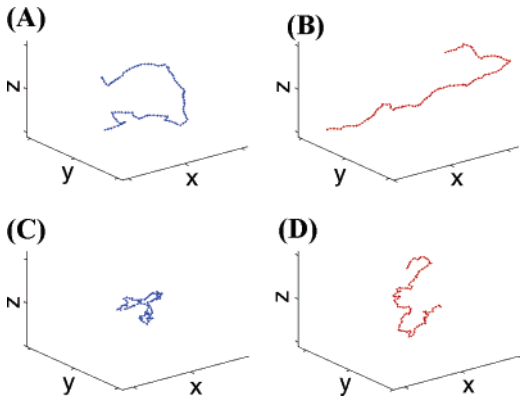

Figure 3. (A, B) Typical conformations of a 100-segment homopolymer with 15 defects generated by MC simulations without (top left) and with (top right) a liquid crystal environment. (C, D) Corresponding conformations for a polymer with 50 defects.

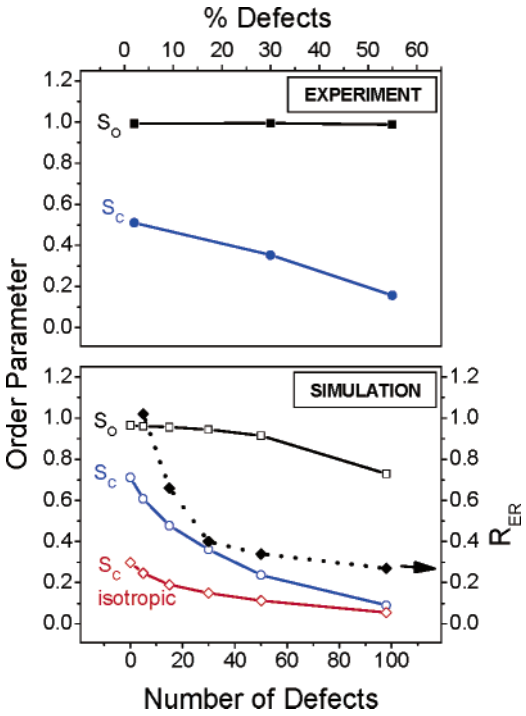

Figure 4. External (S_O) and internal (S_C) order parameters as a function of defect concentration for the three polymer samples (top). The bottom panel shows the order parameters for the simulated polymers as a function of defects including the modified extension ratio and the internal order parameter for chains simulated without the LC potential. The lines only serve as a visual guide.

For the theoretical framework applied herein, S_C and P_{chain} are simply related by $P_{chain} = 3S_C/(2 + S_C)$. Simulated conformational order parameters and orientational order parameters are summarized in Figure 4 (bottom) verifying the expected decrease in both types of order with increasing number of segments. Most striking are the large values for both order parameters even for the polymers with a large number of segments. Figure 4 (bottom) also portrays the modified extension ratio R_{ER} for the chains, which we define as the equilibrium end-to-end distance $\langle r^2 \rangle^{1/2}$ in the LC environment normalized by the end-to-end distance of a purely elongated but nonbent chain. The simulated polymer chain with five defects in fact approaches the fully unbent,

fully elongated limit ($R_{ER} = 1$) indicating the ability of the nematic environment to actually stretch the chain with a small number of defects (assumed to be equally distributed along the chain). It should be noted however that for a highly segmented polymer, such as that shown in Figure 3D, the nematic environment can align segments of the polymer without elongating the polymer by forming hairpin turns in the chains, which when induced by single bond defects have little energy penalty over more elongated defect geometries, e.g., a chain zigzag. A similar interplay between the anisotropic solvation and the intrinsic flexibility of main-chain nematic polymers with flexible spacers between mesogenic groups has previously been inferred from small angle neutron scattering[14] and viscosity[15,16] measurements.

The bottom panel in Figure 4 shows that the simulated orientational order parameters are much greater than the conformational order parameters, demonstrating that the chains are well aligned along the nematic axis and the predicted P values primarily reflect conformational order. The decreases in S_O with decreasing S_C can be traced in this model to the direct dependence of the solvation energy per molecule on S_C as follows

$$V_{chain}(\alpha) = -\frac{3}{2} N_{RU} \nu_{RU} S_C \cos^2 \alpha \left\langle \frac{3}{2} \cos^2 \gamma - \frac{1}{2} \right\rangle \quad (3)$$

where N_{RU} is the number of repeat units per chain. The solid lines in Figure 1 show a best fit (not a simulation) of the model implied by eqs 1 and 3 to the experimental data giving excellent agreement. The top panel of Figure 4 summarizes the order parameters obtained from the fit. This comparison of model and experiment also indicates that the orientational order is much greater than the conformational order and that increasing segmentation decreases conformational order.

In conclusion, we have used polarization SMS and coordinated simulations to explore how polymer segmentation affects the elongation and alignment of polymer chains in a nematic environment.

Acknowledgment. We gratefully acknowledge P. Burn for providing us with the M98 sample and S. Ramakrishnan for the M70 and M45 samples. D.H. thanks the Environmental Molecular Science Laboratory at PNNL for computing resources. G.D.S. acknowledges support from the Natural Sciences and Engineering Research Council of Canada and P.F.B. from the National Science Foundation, Keck Foundation, and Welch Foundation.

References

(1) Onsager, L. *Ann. N. Y. Acad. Sci.* **1949**, *51*, 627.
(2) Lekkerkerker, H. N. W.; Coulon, P.; Van Der Haegen, R.; Deblieck, R. *J. Chem. Phys.* **1984**, *80*, 3427.
(3) Dogic, Z.; Zhang, J.; Lau, A. W. C.; Aranda-Espinoza, H.; Dalhaimer, P.; Discher, D. E.; Janmey, P. A.; Kamien, R. D.; Lubensky, T. C.; Yodh, A. G. *Phys. Rev. Lett.* **2004**, *92*, 125503.
(4) Lammi, R. K.; Fritz, K. P.; Scholes, G. D.; Barbara, P. F. *J. Phys. Chem. B* **2004**, *108*, 4593.
(5) Padmanaban, G.; Ramakrishnan, S. *J. Am. Chem. Soc.* **2000**, *122*, 2244.
(6) Fritz, K. P.; Scholes, G. D. *J. Phys. Chem. B* **2003**, *107*, 10141.
(7) Woo, H. S.; Lhost, O.; Graham, S. C.; Bradley, D. D. C.; Friend, R. H.; Quattrocchi, C.; Bredas, J. L.; Schenk, R.; Muellen, K. *Synth. Met.* **1993**, *59*, 13.
(8) Salamon, Z.; Skibinski, A. *Mol. Cryst. Liq. Cryst.* **1983**, *90*, 205.
(9) Forkey, J. N.; Quinlan, M. E.; Goldman, Y. E. *Prog. Biophys. Mol. Biol.* **2000**, *74*, 1.
(10) Chang, W.-S.; Link, S.; Hu, D.; Barbara, P. F. To be published.
(11) Hu, D. H.; Yu, J.; Wong, K.; Bagchi, B.; Rossky, P. J.; Barbara, P. F. *Nature* **2000**, *405*, 1030.
(12) Hu, D. H.; Yu, J.; Padmanaban, G.; Ramakrishnan, S.; Barbara, P. F. *Nano Lett.* **2002**, *2*, 1121.
(13) Szabo, A. *J. Chem. Phys.* **1980**, *72*, 4620.
(14) D'Allest, J. F. D.; Maissa, P.; ten Bosh, A.; Sixou, P.; Blumstein, A.; Blumstein, R.; Teixeira, J.; Noirez, L. *Phys. Rev. Lett.* **1988**, *61*, 2562.
(15) Chen, F.-L.; Jamieson, A. M. *Macromolecules* **1994**, *27*, 4691.
(16) Chiang, Y.-C.; Jamieson, A. M.; Campbell, S.; Tong, T. H.; Sidocky, N. D.; Chien, L. C.; Kawasumi, M.; Percec, V. *Polymer* **2000**, *41*, 4127.

NL051108L